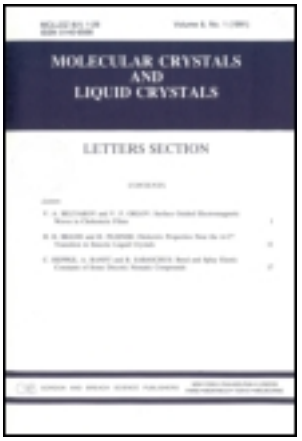

Molecular Crystals and Liquid Crystals
Publication details, including instructions for authors and subscription information:
http://www.tandfonline.com/loi/gmcl20

Organic Light-Emitting Diode Outcoupling Enhancement Using Buffer Layers

Ho-Nyeon Lee [a], Hyun Jun Cho [b] & Doo Hoon Kim [b]
[a] Department of Display and Electronic Information Engineering, Soonchunhyang University, Asan, 336-745, Korea
[b] Department of Electric & Robotics Engineering, Soonchunhyang University, Asan, 336-745, Korea
Published online: 16 Dec 2013.

To cite this article: Ho-Nyeon Lee, Hyun Jun Cho & Doo Hoon Kim (2013) Organic Light-Emitting Diode Outcoupling Enhancement Using Buffer Layers, Molecular Crystals and Liquid Crystals, 584:1, 37-43, DOI: 10.1080/15421406.2013.849427

To link to this article: http://dx.doi.org/10.1080/15421406.2013.849427

Mol. Cryst. Liq. Cryst., Vol. 584: pp. 37–43, 2013

ISSN: 1542-1406 print/1563-5287 online
DOI: 10.1080/15421406.2013.849427

Taylor & Francis
Taylor & Francis Group

Organic Light-Emitting Diode Outcoupling Enhancement Using Buffer Layers

HO-NYEON LEE,[1,*] HYUN JUN CHO,[2] AND DOO HOON KIM[2]

[1]Department of Display and Electronic Information Engineering, Soonchunhyang University, Asan 336-745, Korea
[2]Department of Electric & Robotics Engineering, Soonchunhyang University, Asan 336-745, Korea

Using a buffer layer under the anode, we studied outcoupling enhancement for organic light-emitting diodes. Monolayers of tungsten oxide and titanium oxide were used as the anode buffer layers. Thin anode buffers such as 25 nm and 50 nm tungsten-oxide layers, and a 15 nm titanium-oxide layer noticeably increased the outcoupling. However, thick buffers decreased the outcoupling. The combined effects of the constructive interference and the creation of additional bound modes explain these behaviors. Therefore, the thickness of the anode buffer layers should be optimized under the upper limit, which creates additional bound modes.

Keywords Buffer; outcoupling; titanium oxide; tungsten oxide

Introduction

Organic light-emitting diodes (OLEDs) are expected to be the next major display technology succeeding liquid crystal displays (LCDs). This is because of their superior viewing characteristics compared with those of LCDs. OLEDs are raising their share rapidly in the mobile display market. Encouraged by the success in the mobile display market; OLEDs are aiming to compete with LCDs in television applications. An improvement of the luminous efficiency of OLEDs is essential for OLEDs to expand their application area into large-size display devices. Therefore, there has been much research on the development of high-performance organic materials and the optimization of the electronic device structures of OLEDs. The internal efficiency was improved considerably through the previous research. However, the improvement for the external efficiency of OLEDs is restricted even with the high-performance organic materials and the well-optimized device structures. Most of the generated light in an OLED device is confined in guided modes such as the organic layer waveguide mode, the indium-tin-oxide (ITO) layer waveguide mode, and the surface plasmon polariton (SPP) mode; approximately 20 % of the generated light is emitted from the OLED device [1–3]. Light outcoupling efficiency is a key factor that determines the external luminous efficiency of OLEDs. There have been researches on various outcoupling

*Address correspondence to Prof. Ho-Nyeon Lee, Department of Display and Electronic Information Engineering, Soonchunhyang University, 646, Eupnae-ri, Shinchang-myeon, Asan 336-745, Korea (ROK). Tel.: (+82)41-530-4703; Fax: (+82)41-530-1548. E-mail: hnlee@sch.ac.kr

enhancement methods such as micro cavities [4,5], photonic crystals [6,7], micro lens arrays [8,9], surface modification [10], and light scattering layers [11,12]. The micro-cavity method is based on the resonance structure composed of mirrors formed at both ends; its light outcoupling characteristics have high wavelength dependency and directivity. This method makes the spectrum and light distribution curves sharp and the viewing angle narrow. The photonic crystal method amplifies the diffraction in a specific direction using periodic uneven structures; its characteristics are highly dependent on the wavelength and the direction. The spectrum and the light distribution curves become sharper, and the directionality of the emitted light becomes stronger when this method is used. The micro lens array is fabricated on the outer surface of the substrate and extracts light from waveguide modes in the substrate through geometrical optics. This may distort the image and reduce the resolution. In addition, this causes image and color changes according to the viewing angle. The surface modification method deforms the internal geometric structure of the light-emitting layer of OLEDs. The fabrication of this method is complex and expensive. In addition, the current–voltage characteristics of OLEDs are degraded when the surface modification method is used. The light scattering layer is fabricated by inserting light scattering structures into the interface between layers with a different refractive index. This method increases the haze. As described above, the structure and cost regarding the light outcoupling methods of previous works are complex and expensive; this has worsened the practicality of the outcoupling methods. With this in mind, we studied an outcoupling method using a simple structure with an easy fabrication process to improve the practicality. The anode buffer, which was located between the anode and the glass substrate of OLEDs, was used to increase the outcoupling efficiency in this work. The anode buffer was fabricated using a single insulating layer to prevent the increase in the complexity of the structure and the fabrication cost. This buffer layer contributes in extracting light from the waveguide modes in the organic and anode layers into the glass substrates; the light outcoupling efficiency is expected to increase through the adoption of this anode buffer layer.

Experiments

Figure 1 shows the schematic diagram of the device structure for this work. The device structure was glass substrate/anode buffer/ITO (150 nm)/N,N'-bis(naphthalen-1-yl)-N,N'-bis(phenyl)-benzidine (NPB) (40 nm)/tris(8-hydroxy-quinolinato)aluminium (Alq3) (60 nm)/LiF (1 nm)/Al (100 nm). 0.5t glass (Eagle-XG, Samsung Corning Precision Materials) was used as the substrate. Tungsten-oxide film and titanium-oxide film were used as the anode buffer layer because of their high refractive index. For the visible light, titanium oxide has 2.4∼2.5 refractive index [13] and tungsten oxide has 1.9∼2.1 refractive index [14,15]. The tungsten-oxide film and the titanium-oxide film were deposited by a radio frequency (RF) sputtering method at room temperature using a WO_3 target and a TiO_2 target, respectively. The sputtering gas was a mixture of argon and oxygen. The ITO anode was deposited using a facing-target sputtering method [16] with RF power. The substrate temperature was 200 °C and the process gas was a mixture of argon and oxygen. Anode patterning was conducted using the wet etch method. After the anode fabrication, the NPB, Alq3, LiF, and Al layer were deposited sequentially using a vacuum thermal evaporation method at room temperature. The patterning was conducted using a shadow mask method. After the fabrication process, the OLED device was encapsulated using a glass lid in nitrogen environment. After the encapsulation process, the current-voltage-luminance characteristics were measured in a dark shielding box.

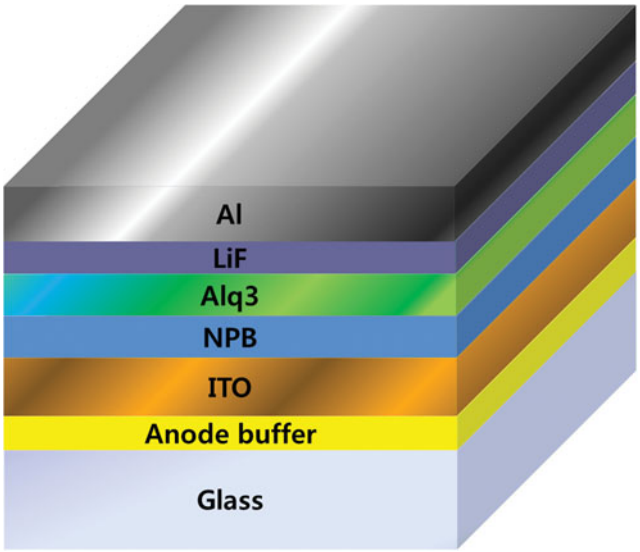

Figure 1. Schematic diagram for the structure of organic light-emitting diodes for this work.

Results and Discussion

Figure 2 shows the luminance of OLEDs with tungsten-oxide anode buffers according to the tungsten-oxide thickness. In each figure (Fig. 2(a)–(d)), the OLED with the tungsten oxide layer of a specific thickness and the OLED without an anode buffer were compared. Both OLEDs were fabricated at the same time using the same process except the fabrication process of the anode buffer; through this comparison method, we could reduce the errors in the analysis of experimental results. As shown in the figure, OLEDs having 25 nm and 50 nm thick tungsten-oxide anode buffers demonstrated higher luminance than that of OLEDs without an anode buffer layer. However, 75 nm and 100 nm thick tungsten-oxide anode buffer layers reduced the luminance of OLEDs. The ratio of the luminance of OLED with the anode buffer (L_{WB}) to the luminance of OLED without an anode buffer (L_{WOB}) is shown in Fig. 2(e). As described above, the anode buffers of thickness 25 nm and 50 nm enhance the ratio but the anode buffers of thickness 75 nm and 100 nm worsen the ratio.

Figure 3 illustrates the current efficiency curves of OLEDs with titanium-oxide anode buffers according to the thickness of the anode buffers. In each figure (Fig. 3(a)–(c)), we compared the current efficiency curves of the OLEDs with a titanium-oxide anode buffer of specific thickness and the OLED without an anode buffer. Each set of OLEDs was fabricated using the same process at the same time, except the fabrication process of anode buffer layers. As shown in the figure, the OLEDs with a 15-nm thick titanium-oxide anode buffer had higher current efficiency than that of OLEDs without an anode buffer layer. However, 25 nm and 70 nm thick titanium-oxide anode buffer layers reduced the current efficiency of OLEDs.

For the tungsten-oxide anode buffer layers, the devices with 25 nm or 50 nm anode buffers demonstrated higher luminance and the device with a 100 nm anode buffer showed lower luminance than the device without an anode buffer. If the interference effect is the reason for these results, 25 nm and 50 nm anode buffers correspond to the constructive interference conditions. The refractive index of tungsten oxide for green light is about 2.0

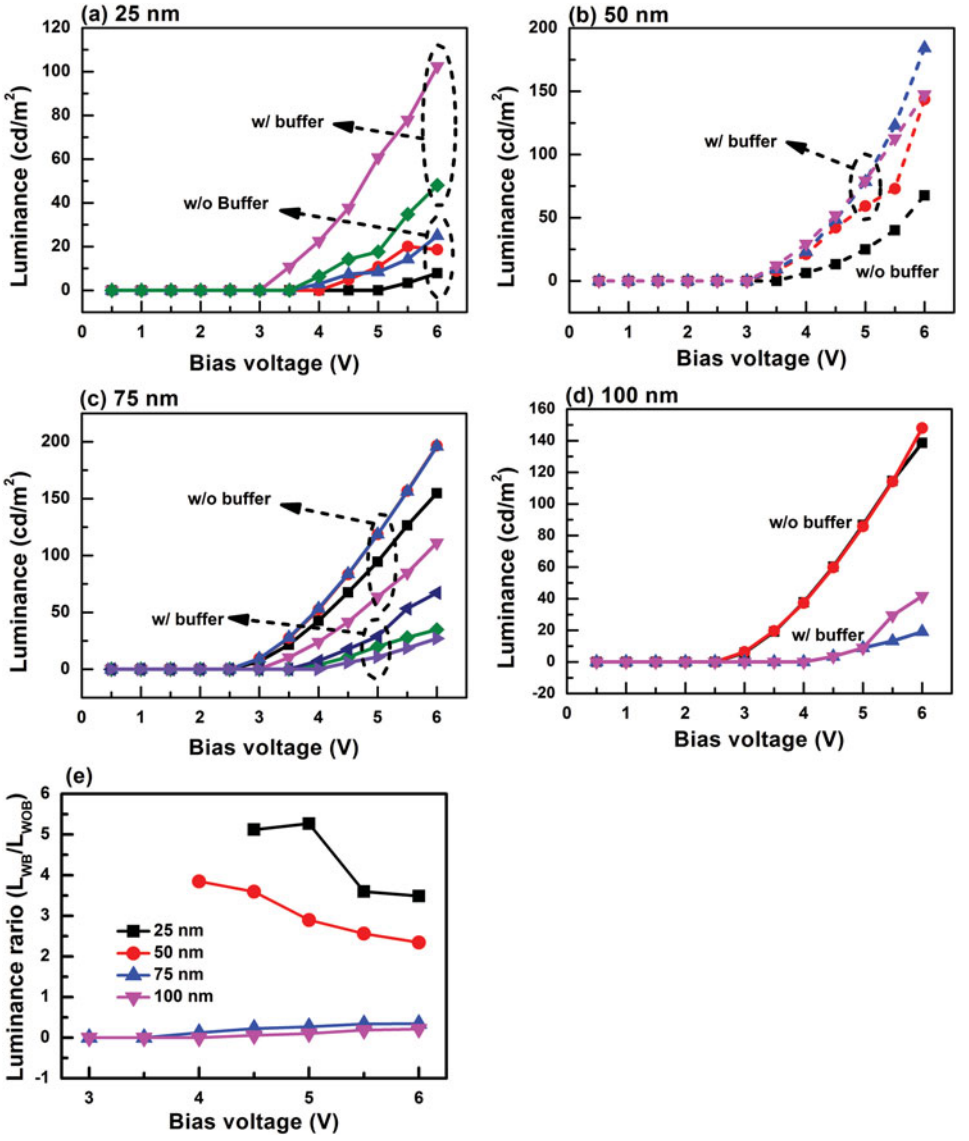

Figure 2. Luminance curves as a function of bias voltage according to the thickness of the tungsten-oxide anode buffer layer; the thickness of anode buffer was (a) 25 nm, (b) 50 nm, (c) 75 nm, and (d) 100 nm, respectively. In (a) ∼ (c), results from OLEDs without an anode buffer were shown for comparison. The ratio of the luminance of OLED with the anode buffer (L_{WB}) to the luminance of OLED without an anode buffer (L_{WOB}) is shown in (e).

[14,15]. Therefore, for 25 nm and 50 nm anode buffers, the optical-path-length difference between a light that penetrates the anode buffer without reflection and a light that get through the anode buffer after pairs of reflections is approximately the integer times of the wavelength of the emitted light. In this case, the 100 nm buffer should also correspond to the constructive condition because 100 nm is an integer multiple of 25 nm and 50 nm.

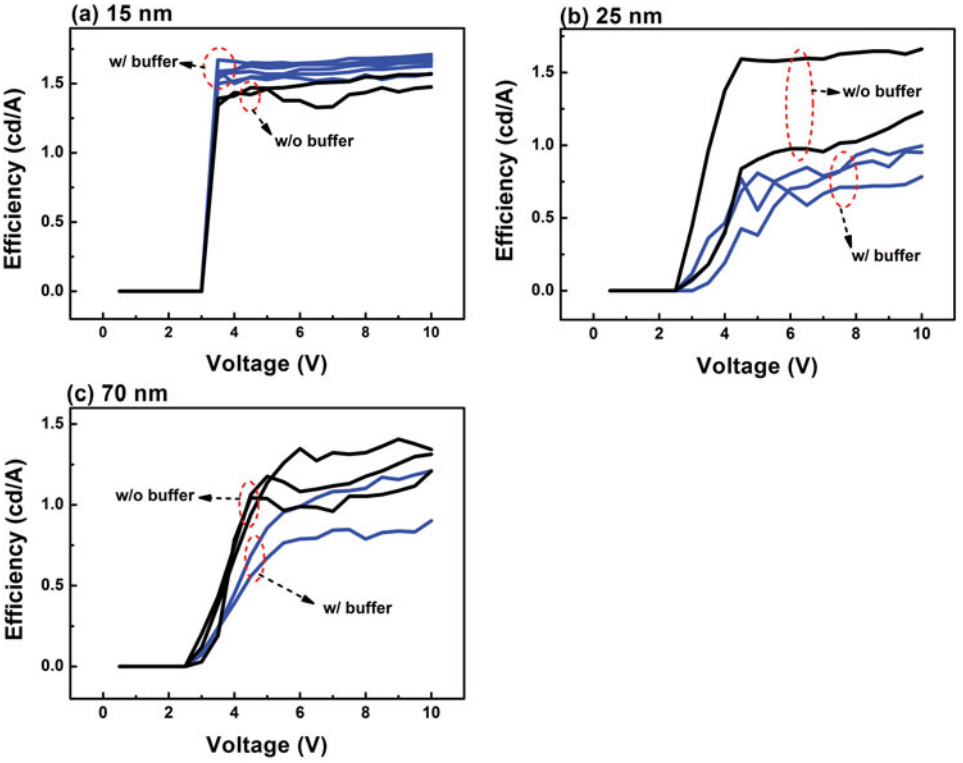

Figure 3. Current efficiency curves as a function of bias voltage according to the thickness of the titanium-oxide anode buffer layer; the thickness of anode buffer was (a) 15 nm, (b) 25 nm, (c) and 70 nm, respectively. In each figure, results from OLEDs without an anode buffer were shown for comparison.

However, the OLED with the 100 nm tungsten-oxide anode buffer showed reduced luminance compared with the device without an anode buffer. Therefore, the interference effect alone cannot explain these results.

Figure 4 shows the simulation results of bound modes in the OLED devices. The simulated device structure was the same as the experimentally fabricated device. The anode buffer was simulated using a pure dielectric material with the refractive index of 2.2. The simulation was performed using a commercial tool (MODE solutions, Lumerical). The OLEDs with a thin anode buffer (Fig. 4(b)) and without an anode buffer (Fig. 4(a)) have three bound modes. However, the OLED with a thick anode buffer (Fig. 4(c)) has five bound modes. The additional bound modes of Fig. 4(c) have peaks in the anode buffer. These additional bound modes can be related with the reduction of the outcoupling of OLEDs with thick anode buffers (Figs. 2 and 3).

From the results of Figs. 2, 3 and 4, thin anode buffer layers increase the outcoupling efficiency of OLEDs; however, thick anode buffer layers decrease the outcoupling efficiency. Constructive interference may be the reason that increased the outcoupling. The optical path lengths of 25 nm and 50 nm thick tungsten-oxide layers approximate the integer times of the center wavelength regarding the electroluminescence spectrum of Alq3. Therefore, the constructive interference may result in improved luminescence. For thicker

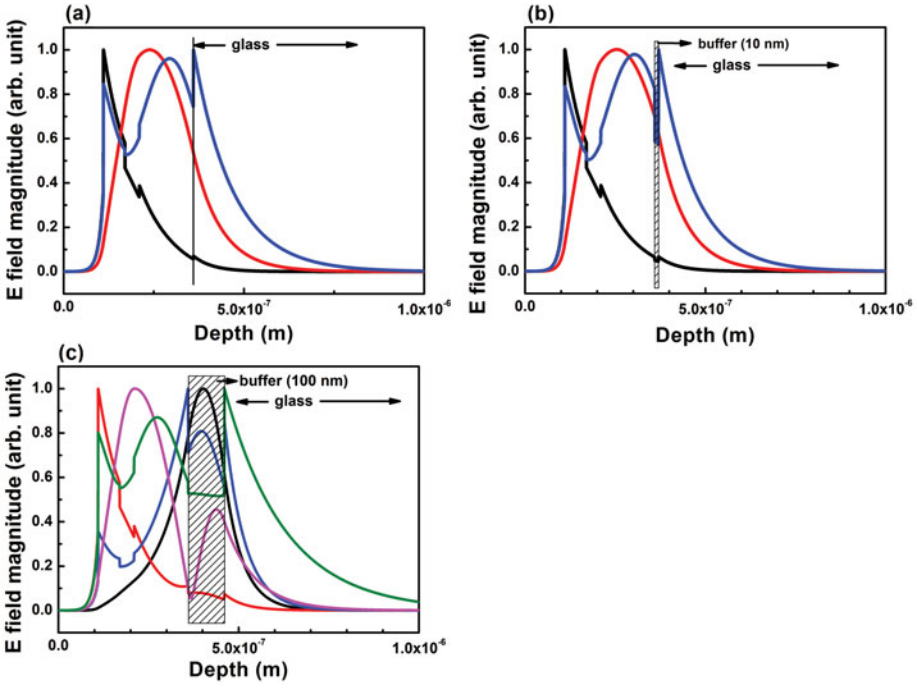

Figure 4. Bound modes inside the OLEDs according to the thickness of the anode buffer layer; the thickness was (a) 0 nm, (b) 10 nm, and (c) 100 nm. The refractive index of the anode buffer layer was 2.2.

anode buffer layers, additional bound modes are created. These additional bound modes can reduce the outcoupling efficiency; OLEDs with thicker anode buffers of tungsten oxide and titanium oxide have reduced outcoupling.

Conclusions

We studied the light outcoupling enhancement method using a single anode buffer layer with various thicknesses. Tungsten oxide and titanium oxide were used as the anode buffer materials. Thin anode buffer layers had an effect on increasing the outcoupling efficiency. However, thick anode buffer layers decreased the outcoupling efficiency. Both 25 nm and 50 nm thick tungsten-oxide and 15 nm thick titanium-oxide films increased the outcoupling; a constructive interference is estimated to cause this increase. OLEDs with thick anode buffers have more bound waveguide modes compared to OLEDs with thin anode buffers as well as OLEDs without an anode buffer. The additional bound modes are expected to cause the reduction in outcoupling. As described above, the anode buffer layers are beneficial for the increase of the light outcoupling of OLEDs. However, the thickness of the anode buffer layers should be restricted to less than the value that creates additional bound modes.

Acknowledgments

This work was supported by the IT R&D program of MKE/KEIT (10041062, Development of fundamental technology for light extraction of OLED) and by the Soonchunhyang University Research Fund.

References

[1] Nowy, S., Frischeisen, J., & Brütting, W. (2009). *Proc. of SPIE*, *7415*, 74151C.
[2] Hong, K., & Lee, J.-L. (2011). *Electron. Mater. Lett.*, *7*, 77.
[3] Chutinan, A., Ishihara, K., Asano, T., Fujita, M., & Noda, S. (2005). *Org. Electron.*, *6*, 3.
[4] Cho, T.-Y., Lin, C.-L., & Wu, C.-C. (2006). *Appl. Phys. Lett.*, *88*, 111106.
[5] Meerheim, R., Nitsche, R., & Leo, K. (2008). *Appl. Phys. Lett.*, *93*, 043310.
[6] Do, Y. R., Kim, Y.-C., Song, Y.-W., & Lee, Y.-H. (2004). *J. Appl. Phys.*, *96*, 7629.
[7] Do, Y. R., Kim, Y. C., Song, Y.-W., Cho, C.-O., Jeon, H., Lee, Y.-J., Kim, S.-H., & Lee, Y.-H. (2003). *Adv. Mater.*, *15*, 1214.
[8] Möller, S., & Forrest, S. R. (2002). *J. Appl. Phys.*, *91*, 3324.
[9] Lin, H.-Y., Ho, Y.-H., Lee, J.-H., Chen, K.-Y., Fang, J.-H., Hsu, S.-C., Wei, M.-K., Lin, H.-Y., Tsai, J.-H., & Wu, T.-C. (2008). *Opt. Express*, *16*, 11044.
[10] Koh, T.-W., Choi, J.-M., Lee, S., & Yoo, S. (2010). *Adv. Mater.*, *22*, 1849.
[11] Nakamura, T., Fujii, H., Juni, N., & Tsutsumi, N. (2006). *Opt. Rev.*, *13*, 104.
[12] Bathelt, R., Buchhauser, D., Gärditz, C., Paetzold, R., & Wellmann, P. (2007). *Org. Electron.*, *8*, 293.
[13] Bennett, J. M., Pelletier, E., Albrand, G., Borgogno, J. P., Lazarides, B., Carniglia, C. K., Schmell, R. A., Allen, T. H., Tuttle-Hart, T., Guenther, K. H., & Saxer, A. (1989). *Appl. Optics*, *28*, 3303.
[14] Rottkay, K., Rubin, M., & Wen, S.-J. (1997). *Thin Solid Films*, *306*, 10.
[15] Subrahmanyam, A., & Karuppasamy, A. (2007). *Sol. Energ. Mat. Sol. C*, *91*, 266.
[16] Ma, H., Cho, J.-S., & Park, C.-H. (2002). *Surf. Coat. Tech.*, *153*, 131.